Thin-Shell Thickness of Two-Dimensional Materials

Enlai Gao
Applied Mechanics Laboratory,
Department of Engineering Mechanics,
Center for Nano and Micro Mechanics,
Tsinghua University,
Beijing 100084, China

Zhiping Xu[1]
Applied Mechanics Laboratory,
Department of Engineering Mechanics,
Center for Nano and Micro Mechanics,
Tsinghua University,
Beijing 100084, China;
State Key Laboratory of Mechanics and
Control of Mechanical Structures,
Nanjing University of
Aeronautics and Astronautics,
Nanjing 210016, China
e-mail: xuzp@tsinghua.edu.cn

In applying the elastic shell models to monolayer or few-layer two-dimensional (2D) materials, an effective thickness has to be defined to capture their tensile and out-of-plane mechanical behaviors. This thin-shell thickness differs from the interlayer distance of their layer-by-layer assembly in the bulk and is directly related to the Föppl–von Karman number that characterizes the mechanism of nonlinear structural deformation. In this work, we assess such a definition for a wide spectrum of 2D crystals of current interest. Based on first-principles calculations, we report that the discrepancy between the thin-shell thickness and interlayer distance is weakened for 2D materials with lower tensile stiffness, higher bending stiffness, or more number of atomic layers. For multilayer assembly of 2D materials, the tensile and bending stiffness have different scaling relations with the number of layers, and the thin-shell thickness per layer approaches the interlayer distance as the number of layers increases. These findings lay the ground for constructing continuum models of 2D materials with both tensile and bending deformation.
[DOI: 10.1115/1.4031568]

Keywords: two-dimensional materials, thin-shell model, thickness, tensile stiffness, bending stiffness

A family of 2D materials, including crystalline graphene, hexagonal boron nitride (*h*-BN), transitional-metal oxides and dichalcogenides (MX_2), silica bilayer, and black (α-P) and blue phosphorus (*β*-P), has attracted much attention in recent years because of their fascinating while controllable properties, as well as their patternable geometries that lay the ground for the so-called "nanoengineering" [1–8]. A wide spectrum of applications has been proposed and demonstrated for high-performance nanoelectromechanical devices and functional materials for filtration, separation, and energy storage [1]. For these applications, mechanical behaviors of these materials are of vital importance not only to maintain structural stabilities under mechanical perturbation but also in exploring novel ideas such as strain-, phase-, and interface-engineering [9–11]. One of the most fundamental parameters characterizing mechanical properties of materials is the Young's modulus *Y*, which could be measured by uniaxial tensile tests that provide data for the relation between tensile force *f* and strain *ε*. A thickness *t* has to be defined so that the tensile stiffness $K = f/(w\varepsilon)$ measured experimentally can be related to $Y = f/(wt\varepsilon)$, where *w* is the width of tensile sample. However, for 2D materials with a thickness of single atom, this definition is unambiguous from a geometrical viewpoint. One may consider the material as a plane with vanishing thickness, or use the van der Waals diameter of the atom as the width of sheet. The most common definition is to use the interlayer distance *d* between neighboring monolayer sheets in their layer-by-layer assemblies, which is consistent with the thickness defined for material applications, such as filtration, separation, and intercalation where the interlayer spaces are used for mass transport or storage [12]. For instance, the value of *d* is 0.34 nm for graphene and *h*-BN. In the study of mechanical behaviors, this definition of thickness is intuitive and consistent as one limits the exploration within the tensile deformation of materials. However, it does not work when the bending deformation is taken into account in the same framework of mechanical analysis, which is common as the flexural mode of 2D materials is more accessible by mechanical or thermal perturbation [13,14]. To model the single- or few-layer 2D materials as a mechanical object with both in-plane and out-of-plane elasticity, one could follow the approach proposed by Föppl and von Karman [15], where the in-plane stretching and out-of-plane bending are coupled. These considerations are not specific for single-atom-thick 2D sheet, and similar problems hold as well for 2D materials with more atomic layers, such as MX_2 nanosheets and silica bilayers.

Using the Föppl–von Karman plate theory or the shallow-shell models based on the same idea, single- or few-layer 2D materials in various forms such as sheets, tubules, scrolls, and cones can be modeled [16,17]. In the implementation, the Young's modulus *Y* and the shell thickness t_s can be determined from the measured tensile stiffness $K = Yt_s$ in experiments and the bending stiffness $D = Yt_s^3/[12(1-\nu^2)]$ that can be extracted from mechanical tests or vibrational analysis. Here, ν is the in-plane Poisson's ratio. That is to say, the thin-shell thickness t_s is defined as [13,14]

$$t_s = [12(1-\nu^2)D/K]^{1/2} \tag{1}$$

In the Föppl–von Karman model, the partial differential equations with high nonlinearity are characterized by a dimensionless coupling constant (the "Föppl–von Karman number") $\gamma = KL^2/D$, which can be related to t_s as

$$\gamma = 12L^2(1-\nu^2)/t_s^2 \tag{2}$$

where *L* is the lateral span of 2D structures. Both t_s and γ are the key material parameters characterizing the structural flexibility under mechanical or thermal perturbations.

Following the definition in Eq. (1), the thin-shell thickness t_s for monolayer graphene sheet is 0.06–0.09 nm [13,14]. The discreteness of reported values is caused by difference in the implementation of molecular simulations to calculate *K* and *D*. Apparently, this value of t_s is much smaller than the interlayer spacing $d = 0.34$ nm in graphite and corresponds to a much higher value of γ in prediction, which further leads to scattered values of Young's modulus $Y = K/t_s$ or K/d reported in the literature, known as the Yakobson's paradox [13,14].

Recently, there are rising interests in other 2D materials including MX_2 with three atomic layers, phosphor with buckled-sheet configuration, and few-layer 2D materials. In this work, we will

[1]Corresponding author.

Contributed by the Applied Mechanics Division of ASME for publication in the JOURNAL OF APPLIED MECHANICS. Manuscript received August 21, 2015; final manuscript received September 5, 2015; published online October 1, 2015. Editor: Yonggang Huang.

assess the definition of their thin-shell thickness in this work based on their mechanical properties characterized from our density functional theory (DFT) based first-principles calculations, as well as data reported in the literature. We consider crystalline graphene, *h*-BN, silicene, α-P and β-P, other layered materials such as MoS_2 and bilayer silica, and graphene multilayers.

We use the VIENNA AB INITIO SIMULATION package (VASP) for all DFT calculations. A plane-wave basis set is implemented with an energy cutoff of 600 eV [18]. Projected augmented wave potentials are used for the ion–electron interaction, and the generalized gradient approximation parameterized by Perdew, Burke, and Ernzerhof is applied to the exchange-correlation functional [19]. The Brillouin zone (BZ) is meshed using a $21 \times 21 \times 1$ Monkhorst–Pack grid centered at the gamma point. Structural relaxation is performed for the primitive cell of all 2D materials, using the conjugated-gradient algorithm. These settings are verified to satisfy a criterion of 1 meV/atom for the energy convergence, and thresholds for the force on atom and stress on cell of 0.01 eV/Å and 0.01 GPa. The interlayer distance of the layered 2D materials is calculated by assuming an AB (AA′) interlayer stacking order. The DFT-D3 correction is used to consider interlayer van der Waals interaction [20].

To calculate the tensile stiffness *K*, tensile tests are carried out on a rectangular supercell, by deforming the lattice in one direction and keeping the other lattice constant free to relax. A reduced *k*-point mesh of $10 \times 10 \times 1$ is used for the supercell. To calculate the bending stiffness *D*, two approaches could be taken. In the first one, the single-layer sheet of 2D material is rolled into a cylindrical nanotube with a radius of *R*. Then, *D* could be fitted from the relation $E = D/(2R^2)$ between strain energy density of the tubule *E*, which is the energy density difference between the tubule and sheet form of 2D materials and the radius *R*. Depending on the direction of rolling process in the 2D lattice, the bending stiffness is calculated along the armchair and zigzag directions, respectively. The *k*-mesh for the roll-up tubule is set to $1 \times 1 \times 20$, with 20 special *k*-points sampled along its axis where a supercell is defined. To obtain *D* from the fitting process, we use data for large-radius tubules to avoid the nonlinearity at high curvatures, reaching an accuracy of the estimation below 0.01 eV. In a second approach, we perform density functional perturbation theory (DFPT) based calculations using the VASP and PHONOPY packages [21]. From the calculated phonon dispersions $\omega(q)$, the group velocities of acoustic phonons can be evaluated as $v = \mathrm{d}\omega/\mathrm{d}q$, which are then used to quantify both in-plane and out-of-plane mechanical properties of the 2D materials. The in-plane stiffness calculated in this way is consistent with those obtained in our tensile tests. For the out-of-plane elasticity, we calculate the bending stiffness *D* from the quadratic dispersion of the flexural phonon mode ZA [22], which is

$$\omega^2 = (D/\rho)q^4 \tag{3}$$

Here, ρ is the areal density of mass. Fitting the dispersion $\omega(q)$ using Eq. (3) yields the value of *D*. In practice, we average the values calculated along the different *k*-paths (Γ-K and Γ-M) in the BZ. We apply both the roll-up approach and DFPT calculations to all 2D materials considered in this work, except for MoS_2 and the silica bilayer, for which only the DFPT method is used. These tubular forms of these three-atom-thick 2D materials contain much more atoms in the model and require significantly higher computational cost compared to the single-atom layers. For the single-atom-thick 2D materials, we confirm that these two approaches predict the bending stiffness consistently. Specifically, for graphene, the difference is less than 0.1 eV.

We summarize the structural and mechanical properties of the 2D materials we calculated and those collected from the literature in Table 1, which are consistent with those reported in the literature, if available. The tensile stiffness *K* and bending stiffness *D* are also plotted in Fig. 1(*a*), from which we can see that the values distribute widely between two boundaries in the *D*/*K* ratios. The lower boundary includes values for the 2D sheet with single-atom thickness, such as graphene, *h*-BN, and silicene, while the data for relatively thick silica bilayer align with the upper boundary. The *D*/*K* ratio for MoS_2, α-P, and β-P locates in between. Moreover, one could see that sheets with buckled configurations such as silicene and β-P have lower tensile and bending stiffness, while flat sheets such as graphene, *h*-BN, silica bilayer, and MoS_2 are stiffer. Moreover, the bending stiffness apparently is higher for thicker sheets and the strong chemical bonding in graphene and *h*-BN offers high tensile stiffness. We further plot the calculated results of *D*/*K* and γ as a function of t_s, together with predictions from Eqs. (1) and (2) using a Poisson's ratio $\nu = \sim 0.3$, although the value of ν is different for the 2D materials. This consistency thus indicates that the variation in Poisson's ratios for specific materials (Table 1) is not crucial for the discussion above. The calculated Föppl–von Karman number for these 2D materials with a typical size of 10 μm is $\sim 10^{10}$–10^{11}, which is 2–3 orders higher than γ for an A4 paper, which is estimated to be $\sim 10^8$. This extremely high value of γ clearly indicates the out-of-plane flexibility of 2D crystalline sheets at the micron scale.

With these data available, we can then calculate the effective thickness of 2D sheets t_s, and compare it with the interlayer distance *d* in their layered assemblies. In order to measure their difference, we define a factor of consistency

$$c = t_s/d \tag{4}$$

with an extreme case of $c = 1$ for an identical definition between the thin-shell thickness and interlayer distance. The results from our calculations are presented in Fig. 2, which shows that thick sheets silica and MoS_2 with $d = 6.50$ and 6.15 Å have higher consistency with $c = 60.6\%$ and 48.9%, respectively. In contrast, flat single-atom-thick graphene and *h*-BN sheets have low values of $c = 26.7\%$ and 28.0%. The factor of consistency for buckled β-P is 36.3%, which is between the values for graphene and three-atom-thick MoS_2 sheets. It should be remarked here that the β-P has a hexagonal lattice as graphene, *h*-BN, and silicene, and thus is isotropic in the elastic response. However, the α-P is anisotropic

Table 1 The lattice constant *a*, in-plane tensile stiffness *K*, Poisson's ratio ν, bending stiffness *D*, thin-shell thickness t_s, and interlayer distance *d* for 2D materials

Materials	*a* (Å)	*K* (N/m)	ν	*D* (eV)	t_s (Å)	*d* (Å)
Graphene [14,23–25]	2.45	345.00	0.15	1.46	0.89	3.34
h-BN [7,8,25,26]	2.51	271.00	0.21	1.29	0.94	3.34
Silicene [6,27,28]	3.83	59.70	0.28	0.37	1.05	3.19
MoS_2 [29–32]	3.13	122.30	0.30	6.29	3.01	6.15
Silica	5.31	133.40	0.50	14.40	3.94	6.50
Black phosphorus (α-P) [5,33,34][a]	$a = 3.30$ $b = 4.63$	24.40	0.17	1.51	3.40	5.30
Blue phosphorus (β-P) [5,35]	3.33	68.60	0.11	0.84	1.52	4.20

[a]For the black phosphorus, tensile and bending stiffness are calculated along the zigzag direction. The calculated values are compared to those reported in the literature listed in the table, if available, which are consistent.

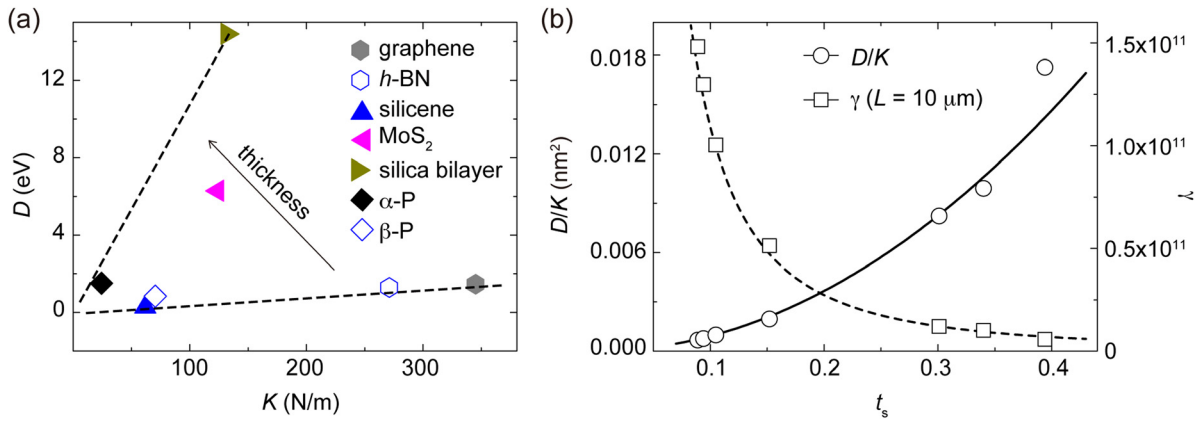

Fig. 1 (*a*) Tensile stiffness *K*, bending stiffness *D*, (*b*) *D*/*K* ratio, and the Föppl–von Karman number γ calculated for 2D materials. For γ, we consider a typical size of 2D materials of 10 μm. The dashed lines in panel (*a*) indicate the boundaries of *D*/*K* ratios, and the solid/dashed lines in panel (*b*) are theoretical predictions with $\nu = 0.3$ based on Eqs. (1) and (2).

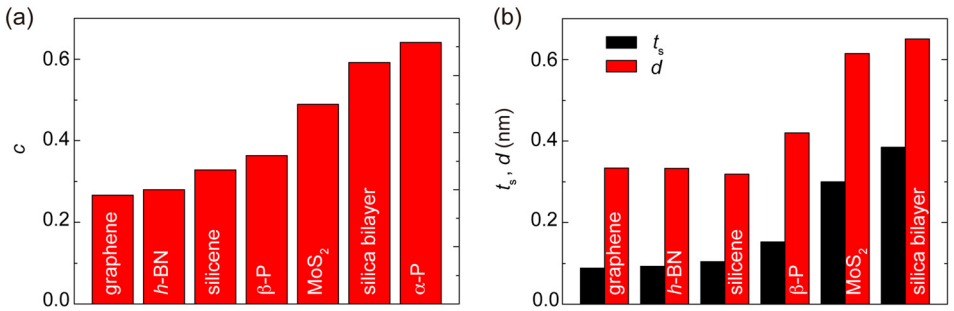

Fig. 2 (*a*) The factor of consistency, *c*, calculated for 2D materials, showing the difference in the definitions of thickness of 2D materials—the thin-shell thickness or interlayer distance in their layer-by-layer assemblies. (*b*) The thin-shell thickness t_s and interlayer distance *d* for 2D materials. The first four 2D materials are single-atom-thick and the last two are few-atom layers.

and is excluded from the data presented in Fig. 2(*b*). Actually, the highly anisotropic nature of α-P and its low tensile stiffness in the tensile zigzag direction lead to a very high value of $c = 64.1\%$. The tensile stiffness in the zigzag direction of α-P is far lower than that along the armchair direction and thus is used to define the thin-shell thickness [5,33,34].

From Fig. 3(*a*) and Table 1, we see that when the bending stiffness of 2D materials is close, the contrast between t_s and d is reduced for those with low tensile stiffness. Additionally, the properties of multilayered 2D materials are now discussed based on the results from DFT calculations [36]. By summarizing the values of thin-shell thickness and interlayer distance in Fig. 3(*b*), we find that the thin-shell thickness t_s approaches the interlayer distance d as the number of layers N increases. This can be explained by the fact that the bending stiffness increases faster with N than the tensile stiffness. As N increases, the tensile stiffness of multilayers increases linearly with N as each layer contributes equally to the resistance to tensile loads. However, the interlayer shear interaction results in interlayer coupling under bending loads and the affinity of deformation increases with N. As a result, the bending stiffness increases nonlinearly with N and approaches an N^3-scaling for large N in the continuum limit [37]. It should be remarked here that in this work, we consider only pure bending deformation of 2D crystals and their layered assemblies as we evaluate D values from DFT calculations. While for transverse bending, additional effect from the interlayer shear that is neglected here has to be included [37].

Our previous discussions can be further extended by exploring the bonding nature in the 2D crystals and its change upon bending deformation of the material. Unlike a plate with macroscopic thickness where asymmetric tension and compression are created on different sides, when single-atom-thick crystals such as graphene and *h*-BN bend, the overlap between π-orbitals on neighboring sites changes asymmetrically on different sides of the sheet, yielding the resistance to bending deformation, while the lack of participation from σ-bonds, which correlates with in-plane stretching and compression deformation, leads to breakdown of the shell theory [36]. For few-atom-thick 2D materials such as silica bilayer and MoS_2, the bending stiffness is contributed also by the in-plane covalent bonds that are compressed and stretched in different atomic layers, leading to the enhancement in bending resistance and a larger factor of consistency. For graphene multilayers, interlayer van der Walls interaction contributes to the load transfer and the graphene layers are compressed or stretched accordingly. As the number of layers increases, the bending resistance arising from σ-bond distortion becomes more dominant compared to the π-orbitals, and this effect explains how t_s approaches the interlayer distance for thick multilayers. These facts explain physics behind the inconsistency between t_s and d defined for 2D materials and their layered assemblies.

To conclude, we calculate the thin-shell thickness of a number of 2D materials from their in-plane tensile stiffness K and out-of-plane bending stiffness D obtained from first-principles calculations. The thin-shell thickness increases with the D/K ratio. Generally, few-atom-layer 2D materials such as MoS_2 and silica have larger thin-shell thickness due to the faster increase of bending stiffness than the tensile stiffness as a function of the number of atomic layers. In multilayered 2D materials, the thin-shell

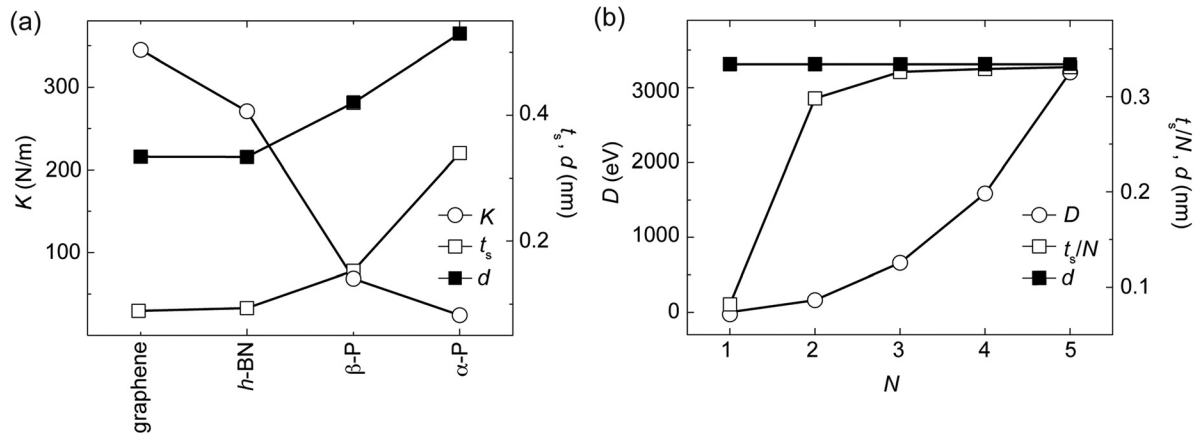

Fig. 3 (*a*) The relation between thin-shell thickness t_s, interlayer distance *d*, and tensile stiffness *K* of 2D materials, where the value of t_s approaches *d* with decreasing *K*. (*b*) The relation between t_s, *d*, and the bending stiffness *D* for graphene multilayers. The value of t_s approaches *d* as the number of layers *N* increases, due to the faster increase of *D* than that of *K* as a function of *N* (data taken from Ref. [36]).

thickness per layer increases with the number of layers and approaches the interlayer distance *d*. These findings are explained by referring to the bonding nature in these 2D materials and their changes upon bending deformation. The data presented in this work and the abovementioned discussions on the thickness of thin-shell models are valuable in developing continuum mechanics models for 2D materials and their derivatives.

Acknowledgment

This work was supported by the National Natural Science Foundation of China through Grant No. 11222217 and the State Key Laboratory of Mechanics and Control of Mechanical Structures, Nanjing University of Aeronautics and Astronautics, through Grant No. MCMS-0414G01. The computation was performed on the Explorer 100 cluster system at the Tsinghua National Laboratory for Information Science and Technology.

References

[1] Butler, S. Z., Hollen, S. M., Cao, L., Cui, Y., Gupta, J. A., Gutiérrez, H. R., Heinz, T. F., Hong, S. S., Huang, J., Ismach, A. F., Johnston-Halperin, E., Kuno, M., Plashnitsa, V. V., Robinson, R. D., Ruoff, R. S., Salahuddin, S., Shan, J., Shi, L., Spencer, M. G., Terrones, M., Windl, W., and Goldberger, J. E., 2013, "Progress, Challenges, and Opportunities in Two-Dimensional Materials Beyond Graphene," ACS Nano, **7**(4), pp. 2898–2926.
[2] Xu, Z., 2011, "Nano-Engineering of Graphene and Related Materials," *Physics and Applications of Graphene*, S. Mikhailov, ed., Intech, Rijeka, Croatia.
[3] Heyde, M., Shaikhutdinov, S., and Freund, H. J., 2012, "Two-Dimensional Silica: Crystalline and Vitreous," Chem. Phys. Lett., **550**, pp. 1–7.
[4] Splendiani, A., Sun, L., Zhang, Y., Li, T., Kim, J., Chim, C. Y., Galli, G., and Wang, F., 2010, "Emerging Photoluminescence in Monolayer MoS_2," Nano Lett., **10**(4), pp. 1271–1275.
[5] Zhu, Z., and Tománek, D., 2014, "Semiconducting Layered Blue Phosphorus: A Computational Study," Phys. Rev. Lett., **112**(17), p. 176802.
[6] Yang, C., Yu, Z., Lu, P., Liu, Y., Ye, H., and Gao, T., 2014, "Phonon Instability and Ideal Strength of Silicene Under Tension," Comput. Mater. Sci., **95**, pp. 420–428.
[7] Michel, K. H., and Verberck, B., 2009, "Theory of Elastic and Piezoelectric Effects in Two-Dimensional Hexagonal Boron Nitride," Phys. Rev. B, **80**(22), p. 224301.
[8] Michel, K. H., and Verberck, B., 2011, "Phonon Dispersions and Piezoelectricity in Bulk and Multilayers of Hexagonal Boron Nitride," Phys. Rev. B, **83**(11), p. 115328.
[9] Xue, K., and Xu, Z., 2010, "Strain Effects on Basal-Plane Hydrogenation of Graphene: A First-Principles Study," Appl. Phys. Lett., **96**(6), p. 063103.
[10] Xu, Z., and Buehler, M. J., 2012, "Heat Dissipation at a Graphene-Substrate Interface," J. Phys.: Condens. Matter, **24**(47), p. 475305.
[11] Duerloo, K.-A. N., Li, Y., and Reed, E. J., 2014, "Structural Phase Transitions in Two-Dimensional Mo- and W-Dichalcogenide Monolayers," Nat. Commun., **5**, p. 4214.
[12] Wei, N., Peng, X., and Xu, Z., 2014, "Understanding Water Permeation in Graphene Oxide Membranes," ACS Appl. Mater. Interfaces, **6**(8), pp. 5877–5883.
[13] Wang, L., Zheng, Q., Liu, J. Z., and Jiang, Q., 2005, "Size Dependence of the Thin-Shell Model for Carbon Nanotubes," Phys. Rev. Lett., **95**(10), pp. 105501–105504.
[14] Huang, Y., Wu, J., and Hwang, K. C., 2006, "Thickness of Graphene and Single-Wall Carbon Nanotubes," Phys. Rev. B, **74**(24), p. 245413.
[15] Landau, L. D., and Lifshitz, E. M., 1986, *Theory of Elasticity*, Butterworth-Heinemann, Oxford, UK.
[16] Yakobson, B. I., Brabec, C. J., and Bernholc, J., 1996, "Nanomechanics of Carbon Tubes: Instabilities Beyond Linear Response," Phys. Rev. Lett., **76**(14), pp. 2511–2514.
[17] Zhang, T., Li, X., and Gao, H., 2014, "Defects Controlled Wrinkling and Topological Design in Graphene," J. Mech. Phys. Solids, **67**, pp. 2–13.
[18] Perdew, J. P., Burke, K., and Ernzerhof, M., 1997, "Generalized Gradient Approximation Made Simple," Phys. Rev. Lett., **78**(7), p. 1396.
[19] Blöchl, P. E., 1994, "Projector Augmented-Wave Method," Phys. Rev. B, **50**(24), pp. 17953–17979.
[20] Grimme, S., Antony, J., Ehrlich, S., Krieg, H., 2010, "A Consistent and Accurate Ab Initio Parametrization of Density Functional Dispersion Correction (DFT-D) for the 94 Elements H-Pu," J. Chem. Phys., **132**(15), p. 154104.
[21] Togo, A., and Tanaka, I., 2005, "First Principles Phonon Calculations in Materials Science," Scr. Mater., **108**, pp. 1–5.
[22] Karssemeijer, L. J., and Fasolino, A., 2011, "Phonons of Graphene and Graphitic Materials Derived From the Empirical Potential LCBOPII," Surf. Sci., **605**(17–18), pp. 1611–1615.
[23] Liu, F., Ming, P., and Li, J., 2007, "Ab Initio Calculation of Ideal Strength and Phonon Instability of Graphene Under Tension," Phys. Rev. B, **76**(6), p. 064120.
[24] Koskinen, P., and Kit, O. O., 2010, "Approximate Modeling of Spherical Membranes," Phys. Rev. B, **82**(23), p. 235420.
[25] Kudin, K. N., Scuseria, G. E., and Yakobson, B. I., ., 2001, "C_2F, BN, and C Nanoshell Elasticity From Ab-Initio Computations," Phys. Rev. B, **64**(23), p. 235406.
[26] Hod, O., 2012, "Graphite and Hexagonal Boron-Nitride Have the Same Interlayer Distance. Why?" J. Chem. Theory Comput., **8**(4), pp. 1360–1369.
[27] Zhao, H. J., 2012, "Strain and Chirality Effects on the Mechanical and Electronic Properties of Silicene and Silicane Under Uniaxial Tension," Phys. Lett. A, **376**(46), pp. 3546–3550.
[28] Fu, H. X., Zhang, J., Ding, Z. J., Li, H., and Meng, S., 2014, "Stacking-Dependent Electronic Structure of Bilayer Silicene," Appl. Phys. Lett., **104**(13), p. 131904.
[29] Molina-Sánchez, A., and Wirtz, L., 2011, "Phonons in Single-Layer and Few-Layer MoS_2 and WS_2," Phys. Rev. B, **84**(15), p. 155413.
[30] Li, T. S., 2012, "Ideal Strength and Phonon Instability in Single-Layer MoS_2," Phys. Rev. B, **85**(23), p. 235407.
[31] Jiang, J. W., Qi, Z., Park, H. S., and Rabczuk, T., 2013, "Elastic Bending Modulus of Single-Layer Molybdenum Disulfide (MoS_2): Finite Thickness Effect," Nanotechnology, **24**(43), p. 435705.
[32] Radisavljevic, B., Radenovic, A., Brivio, J., Giacometti, V., and Kis, A., 2011, "Single-Layer MoS_2 Transistors," Nat. Nanotechnol., **6**(3), pp. 147–150.
[33] Wei, Q., and Peng, X., 2014, "Superior Mechanical Flexibility of Phosphorene and Few-Layer Black Phosphorus," Appl. Phys. Lett., **104**(25), p. 251915.
[34] Wang, Z., and Feng, P. X. L., 2015, "Design of Black Phosphorus 2D Nanomechanical Resonators by Exploiting the Intrinsic Mechanical Anisotropy," 2D Mater., **2**(2), p. 021001.
[35] Guan, J., Jin, Z., Zhu, Z., Chuang, C., Jin, B.-Y., and Tománek, D., 2014, "Local Curvature and Stability of Two-Dimensional Systems," Phys. Rev. B, **90**(24), p. 245403.
[36] Zhang, D. B., Akatyeva, E., and Dumitrică, T., 2011, "Bending Ultrathin Graphene at the Margins of Continuum Mechanics," Phys. Rev. Lett., **106**(25), p. 255503.
[37] Liu, Y., Xu, Z., and Zheng, Q., 2011, "The Interlayer Shear Effect on Graphene Multilayer Resonators," J. Mech. Phys. Solids, **59**(8), pp. 1613–1622.